Solvation dynamics following electron photodetachment from I − in aqueous clusters

M. Dolores Elola and Daniel Laria

Citation: The Journal of Chemical Physics **117**, 2238 (2002); doi: 10.1063/1.1489896
View online: http://dx.doi.org/10.1063/1.1489896
View Table of Contents: http://scitation.aip.org/content/aip/journal/jcp/117/5?ver=pdfcov
Published by the AIP Publishing

Solvation dynamics following electron photodetachment from I^- in aqueous clusters

M. Dolores Elola
Departamento de Química Inorgánica, Analítica y Química-Física e INQUIMAE, Facultad de Ciencias Exactas y Naturales, Universidad de Buenos Aires, Ciudad Universitaria, Pabellón II, 1428, Buenos Aires, Argentina

Daniel Laria
Departamento de Química Inorgánica, Analítica y Química-Física e INQUIMAE, Facultad de Ciencias Exactas y Naturales, Universidad de Buenos Aires, Ciudad Universitaria, Pabellón II, 1428, Buenos Aires, Argentina and Unidad Actividad Química, Comisión Nacional de Energía Atómica, Avenida Libertador 8250, 1429, Buenos Aires, Argentina

(Received 11 February 2002; accepted 7 May 2002)

Equilibrium and dynamical aspects of the earliest stages of solvation following the electronic excitation of I^- dissolved in aqueous clusters were investigated, using a mixed quantum-classical molecular dynamics algorithm. The systems were modeled as composed by an excess quantum charge coupled to a classical bath that includes a neutral iodine and $N_w=6$, 50, and 100 water molecules. In small clusters, the equilibrium solvation structures of the iodine are characterized by surface states that gradually turn into interior states as one considers larger aggregates. Electronic properties of the ground and first excited states are described. In small aggregates, both states are characterized by highly diffuse density profiles that extend well beyond the spatial extent of the aggregates. In larger clusters, the confining potential provided by the classical bath localizes the electron within the aggregates. Dynamical aspects of the solvation relaxation following a vertical excitation of the solute were also examined. In all cases, the relaxation mechanisms involve a global reorganization of the original solvation structure characterized by a gradual stabilization of the solvent-solvent interactions in detriment of a less favorable electron solvation. The overall characteristic time for the solvation is in the order of $\tau_s \approx 0.05$ ps for $N_w=6$ and attains $\tau_s \approx 0.60$ ps for $N_w=100$. [DOI: 10.1063/1.1489896]

I. INTRODUCTION

Absorption spectra of simple aqueous halides provide clear evidence of the strong influence of solvation upon the electronic structure of these probes: In vacuo, the ions do not support bound excited states; only when dissolved in polar media do broad absorption bands appear in the UV region. The stabilization of excited electronic states occurs as the result of the influence of solvent polarization fluctuations that lead to the so-called charge transfer to solvent (CTTS) states.[1,2] In bulk phases, the dynamical characteristics of these fluctuations normally induce the photodetachment of the excess electron from the ion and its subsequent solvation within a solvent cavity, in a time scale of a few picoseconds. Ultrafast time-resolved spectroscopic experiments have revealed that the electron photodetachment mechanisms are far from being simple and present well-differentiated characteristics from those related to the generation of excess electrons in photoionization experiments in neat water.[3–5] From the theoretical point of view, several simulation studies have been performed to investigate the microscopic mechanisms that drive these processes. Sheu and Rossky[6–9] performed a series of molecular dynamics experiments that shed light on the nature of the electronic density of states, absorption spectra, and different reactive channels of photoexcited aqueous iodide; in a similar spirit, Staib and Borgis[10] examined the electronic characteristics of chloride in aqueous solutions as well.

Mesoscopic water clusters represent peculiar polar environments in which the spatial confinement imposed by the finite dimensions of the aggregates—normally on the order of a few nanometers—are translated into large anisotropies in the intramolecular force fields, which, in turn, induce important modifications in the reactive channels from those found in conventional macroscopic phases. In this context, a basic question emerges related to the minimum number of water molecules required to stabilize CTTS precursor states. Combariza *et al.*[12] have performed *ab initio* calculations of several minimum-energy configurations of $X^-(H_2O)_n$ clusters ($X=$Cl, Br, and I) and determined that the threshold number is 6. However, Serxner *et al.*[11] performed electron photodetachment experiments that would indicate the presence of very diffuse, dipole-bound states in clusters as small as $I^-(H_2O)_2$. Moreover, these experiments clearly show the gradual blue shift in the spectrum maxima from ≈4 eV for $n=2$ up to ≈4.5 eV for $n=4$, with a limiting bulk value of ≈5.5 eV. These experimental findings have been corroborated by more recent and comprehensive *ab initio* computational studies of CTTS precursor states.[13,14]

Femtosecond photoelectron spectroscopy studies of $I^-(D_2O)_n$ and $I^-(NH_3)_n$ clusters have been performed by

Newmark and collaborators.[15,16] Using pump and probe techniques, these experiments provide information of the topology of the first excited electronic state potential energy surfaces. The two types of clusters exhibit well-differentiated dynamical features during the early stages of the solvation following the photoexcitation of the solute. The $n=6$ cases are the most illustrative: Results from time-dependent vertical detachment energies (VDE's) in water clusters suggest that the excited-state dynamics includes a solvation-induced isomerization between two stable structures in the cluster. This interconversion would take place on a time scale of $\approx$250–500 fs and would lead from a dipole bound solvation state to a solvation structure similar to that of the stable ground state of $(H_2O)_6^-$. On the other hand, the characteristics of the early stages of the solvation dynamics in ammonia clusters would correspond to a single relaxation which tends towards a gradually more stable solvation of the excess electron.

The experimental findings described in the previous paragraphs represent the main motivations of the present study where we examine dynamical aspects of the early stages of the solvation following a vertical electronic excitation of I^- in aqueous clusters using molecular dynamics techniques. In order to maintain a computationally tractable methodology, the inherently quantum mechanical description of the dynamics has been very much simplified and relies on models developed in earlier studies of similar reactions in bulk phases.[6–10] We first considered the equilibrium solvation structures of different clusters, spanning a size interval that allowed us to investigate both surface and interior states of the solute. Moreover, we also investigated how these solvation structures affect the characteristics of the electronic densities of states and absorption spectra. From a dynamical point of view, we focused our attention on acquiring a first qualitative insight into the mechanisms that drive the early stages of the solvation and on obtaining estimates for the overall characteristic times for the solvation. In particular, we put special emphasis on identifying the effects imposed by both the confinement and presence of the cluster free surface on dynamical aspects of the spatial localization of the excess electron following the vertical photoexcitation of the probe.

The outline of the paper is as follows. In Sec. II we provide a brief description of the model and the methodology used to run the simulations. Section III includes results for equilibrium solvation structures and details of the densities of electronic states and absorption spectra for different cluster sizes. Section IV considers dynamical relaxations of the solvation structures and other relevant electronic parameters following the excitation of the probe. The conclusions of the paper are presented in Sec. V.

II. MODEL AND SIMULATION METHODS

The systems under investigation consisted of one iodide dissolved in aqueous clusters containing $N_w=6$, 50, and 100 molecules. Our description of the solute is similar to that adopted in previous simulation studies of photodetachment processes in bulk water[6–10] and is based on a hybrid quantum-classical approach, in the adiabatic Born-Oppenheimer approximation. Within this simplified picture, I^- is modeled as an excess electron interacting with a neutral iodine atom via a one-electron model pseudopotential. In addition, effects of the different environments on the electronic distribution are taken into account via a second effective interaction between the excess charge and the rest of the water molecules. Quantum fluctuations are neglected for all particles with the exception of the excess electron.

The potential energy between the classical particles $V_{\mathrm{cl}}(\{\mathbf{R}_N\})$ comprises two major contributions: a water-water interaction term that was modeled using the TIP4P model[17] and a water-iodine interaction that was taken to be the sum of standard (6–12) Lennard Jones pair contributions.[6] The electron-iodine pseudopotential V_{eI} was taken from Ref. 6 and represents the effective interaction of the outer $5p$ electron with the iodine nucleus partially shielded by its core and valence electrons. In the absence of solvent, this model pseudopotential presents four bound states: one with *s*-like characteristics and three *p*-like degenerate states, one of which will be occupied by the tagged single electron. Henceforth, we will denote this state as the ground state of I^-.

The coupling between the electron and the classical water molecules, V_{ew}, was considered to be the sum of electron-solvent site pair contributions of the type

$$V_{ew}(\mathbf{r};\{\mathbf{R}_{N_w}\})=-\sum_{i=1}^{N_w}\sum_{\alpha} Q_\alpha e\frac{\mathrm{erf}(\kappa_\alpha|\mathbf{r}-\mathbf{R}_\alpha^i|)}{|\mathbf{r}-\mathbf{R}_\alpha^i|}, \qquad (1)$$

where e represents the electron charge; $\mathbf{R}_\alpha^i$ and Q_α identify the coordinates and the partial charge of site $\alpha=(\mathrm{O,H,H})$ in the ith water molecule, respectively. A similar functionality form for V_{ew} has been implemented in previous studies of excess electrons in polar media[10,18] and corresponds to a Coulomb interaction between the excess charge and Gaussian-distributed partial charges centered at the atomic positions of the water molecules. The spread parameters κ_α^{-1} were adjusted so as to obtain reasonable agreement between the computed energies for several local minima of the TIP4P anion cluster $(H_2O)_6^-$ and the results obtained with more refined quantum calculations. The optimized parameters were found to be $\kappa_{\mathrm{O}}=0.766\ \text{Å}^{-1}$ and $\kappa_{\mathrm{H}}=0.832\ \text{Å}^{-1}$; with the latter values, the computed VDE's for *T*-like and *Y*-like local minimum structures of the $(H_2O)_6^-$ were found to be 0.45 eV and 0.32 eV, respectively. These energy values compare reasonably well with more accurate density functional theory results that yield VDE's ranging from 0.45 eV to 0.51 eV for different *T*-like structures and intermediate values between 0.28 eV and 0.46 eV for *Y*-like local minimum structures.[19]

A. Adiabatic dynamics

We shall now briefly describe the simulation procedure. Consider an initial configuration of the classical particles $\{\mathbf{R}_N\}$; for this particular configuration, we solve the one-electron Schrödinger equation

$$\hat{H}_e\psi_n(\mathbf{r};\{\mathbf{R}_N\})=E_n(\{\mathbf{R}_N\})\psi_n(\mathbf{r};\{\mathbf{R}_N\}), \qquad (2)$$

where $\hat{H}_e$ represents the electronic Hamiltonian:

$$\hat{H}_e = -\frac{\hbar^2}{2m_e}\nabla_{\mathbf{r}}^2 + \hat{V}_{es}(\hat{\mathbf{r}};\{\mathbf{R}_N\}). \tag{3}$$

In the previous equations, $\mathbf{r}$ denotes the electron coordinates, m_e is the electron mass, $2\pi\hbar$ is the Planck constant, and $\hat{V}_{es} = \hat{V}_{eI} + \hat{V}_{ew}$ represents the coupling between the electron and the classical bath. The hypothesis of adiabatic dynamics implies that the quantum forces that drive the dynamics of the classical nuclei are computed exclusively from E_n, the nth instantaneous eigenstate of the electronic Hamiltonian (the choice of the particular quantum state n will be discussed below). The resulting Hamiltonian for the classical particles with masses $\{M_j\}$ is given by

$$H(\{\mathbf{R}_N\}) = \sum_j \frac{M_j\dot{\mathbf{R}}_j^2}{2} + E_n(\{\mathbf{R}_N\}) + V_{\mathrm{cl}}(\{\mathbf{R}_N\}), \tag{4}$$

which leads to the following Newtonian equation of motion of the ith classical particle:

$$M_i\ddot{\mathbf{R}}_i(t) = -\nabla_{\mathbf{R}_i}E_n(\{\mathbf{R}_N(t)\}) - \nabla_{\mathbf{R}_i}V_{\mathrm{cl}}(\{\mathbf{R}_N(t)\}). \tag{5}$$

Two different sets of simulation experiments were performed. The first one involved series of 500 ps molecular dynamics runs corresponding to the microcanonical ensemble in which the quantum forces on the classical particles were taken with the electron occupying the instantaneous ground state of $\hat{H}_e$. The average temperature of the classical particles along these runs was adjusted to $T \approx 200$ K. In large clusters, this corresponds to a thermal regime where the systems present dynamical characteristics similar to macroscopic liquid phases. The second kind of experiments corresponded to nonequilibrium trajectories: Initial states were sampled from configurations generated by the microcanonical trajectory and separated by 5 ps intervals; this time was sufficiently long to yield statistically independent conditions. At $t=0$, the dynamics was modified and the quantum forces were computed according to Eq. (5) using the instantaneous first excited electronic state. From these initial conditions we followed the solvent relaxations for approximately 1 ps.

To solve the Schrödinger equation [cf. Eq. (2)] we found it convenient to expand the electronic wave function in terms of a mobile spherical Gaussian basis set with fixed widths:

$$\psi_n(\mathbf{r};\{\mathbf{R}(t)\}) = \sum_{i=1}^{N_b} c_i^n(\{\mathbf{R}(t)\})\phi_i(\mathbf{r}), \tag{6}$$

$$\phi_i(\mathbf{r}) = \left(\frac{2\alpha_i}{\pi}\right)^{3/4} e^{-\alpha_i(\mathbf{r}-\mathbf{r}_i)^2}; \tag{7}$$

in the previous equation, $\mathbf{r}_i$ denotes the coordinates of the center of the ith basis. Following Ref. 10, the centers of the Gaussian basis were located at the vertices of regular polyhedra situated in concentric shells of increasing radii R_i, centered at the instantaneous position of the iodine, $\mathbf{R}_{\mathrm{I}}(t)$. Using this geometrical distribution, the resulting electronic wave function can be pictured as a linear superposition of s-, s/p-, and $s/p/d$-like orbitals. s-like orbitals are approximately represented by basis centered at $\mathbf{R}_I$, while s/p and $s/p/d$ orbitals are represented by 4 and 12 bases located at the vertices of regular tetrahedra and icosahedra, respectively. In order to provide sufficient flexibility in the description of the ground (localized) and excited (highly diffuse) electronic states, a total of $N_b = 208$ bases—some of them lying well beyond the position of the classical water molecules—was required. Convergence tests for the chosen basis set were performed on several configurations along the simulation runs by including additional polyhedra; moreover, for all cluster sizes investigated, we found no need to supplement the set with mobile basis centered at the instantaneous maximum of the electron density.[20] Full details of the optimized geometrical parameters of the different basis can be found in Table I. The implementation of a Gaussian basis set, along with the adopted functional forms of the different contributions to V_{es}, permitted the analytical evaluation of all matrix elements required for the calculation of the basis set coefficients $\{c_i^n\}$ and for the computation of the quantum forces as well.

III. EQUILIBRIUM PROPERTIES

A. Solvation structures of I^-

The characteristics of the electronic dynamics following the photoexcitement of I^- will be very much dependent on the nature of the original ground and excited electronic states of the solute prior to the excitation, which, in turn, are affected in a sensible way by the solvation structure provided by the particular environment considered. The gross features to analyze are whether the solute resides, on average, in the interior or near the surface of the clusters and at which threshold cluster size the transition from *surface* to *bulk* state occurs. Solvation structures in ionic clusters of the types

TABLE I. Basis set parameters.

Atomic orbital	$\alpha_i^{-1/2}$ (Å)	R_i (Å)
s	0.01	0.0
	0.02	0.0
	0.05	0.0
	0.09	0.0
s/p	0.04	0.005
	0.09	0.009
	0.17	0.017
	0.26	0.026
	0.29	0.029
	0.41	0.041
	0.68	0.068
	0.70	0.120
	1.67	0.167
$s/p/d$	0.62	0.2
	2.4	0.5
	5.3	1.7
	6.3	2.0
	9.5	3.0
	13.0	4.0
	16.0	5.0
	19.0	6.0
	22.0	7.0
	32.0	10.0
	45.0	13.0
	71.0	21.0
	79.0	25.0
	100.0	30.0

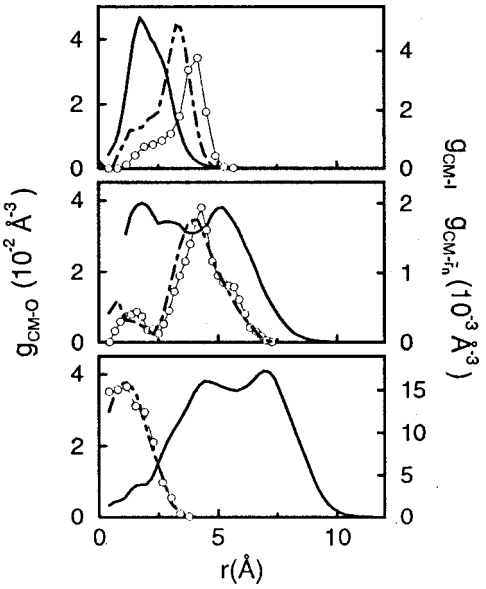

FIG. 1. Radial distribution functions from the cluster center of mass for clusters of different sizes. Top panel: $N_w=6$. Middle panel: $N_w=50$. Bottom panel: $N_w=100$. $g_{\text{c.m.-O}}(r)$: solid line (left hand axis). $g_{\text{c.m.-I}}(r)$: dash-dotted lines (right hand axis). $g_{\text{c.m.-}\bar{r}_1}(r)$: circles (right-hand axis). Results for $g_{\text{c.m.-}\bar{r}_0}$ are indistinguishable from those of $g_{\text{c.m.-I}}$.

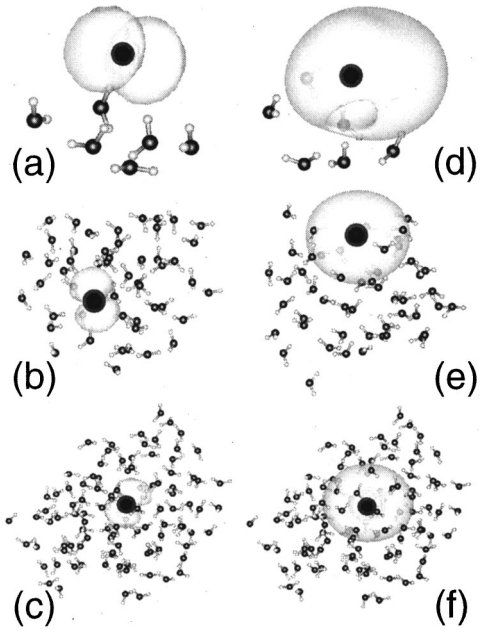

FIG. 2. Isodensity profiles for the ground [(a), (b), (c); $|\psi_0|^2=0.01$ Å^{-3}] and first excited states [(d), (e), (f); $|\psi_1|^2=0.015$ Å^{-3}] of I^- dissolved in aqueous clusters. Top panels: $N_w=6$. Middle panels: $N_w=50$. Bottom panels: $N_w=100$. The position of the iodine is denoted by the black circle.

$M^+(H_2O)_n$ and $X^-(H_2O)_n$—with M (X) an alkaline metal (halogen)—have been investigated in several simulation experiments, incorporating an increasing degree of sophistication in the effective interactions.[21] The picture that emerges from these studies is that the resulting solvation structures seem to be very much dependent on subtle details of the specific Hamiltonian considered. Anyhow, to the best of our knowledge, these results still await proper corroboration from direct experimental measurements.[22]

Useful quantities to consider in this connection are the spatial correlation functions with respect to the cluster center of mass, $g_{\text{c.m.-}\alpha}(r)$, defined as

$$g_{\text{c.m.-}\alpha}(r)=\frac{1}{4\pi r^2}\sum_{i=1}^{N_\alpha}\langle\delta(|\mathbf{R}_\alpha^i-\mathbf{R}_{\text{c.m.}}|-r)\rangle, \tag{8}$$

which give the probability of finding an atom of species α at a distance r from the cluster center of mass located at $\mathbf{R}_{\text{c.m.}}$. In the previous equation, $\langle\cdots\rangle$ denotes a time average over microcanonical trajectories. In Fig. 1 we present results for $g_{\text{c.m.-}\alpha}(r)$, $\alpha=$O, I. Several features are worth commenting: First, one can observe a gradual transition from *surface*- to *bulk*-like solvation as we move from $N_w=6$ to $N_w=100$. For $N_w=6$, the solvation structure of the iodide is clearly asymmetric with respect to the overall spatial distribution of the water molecules. The typical configuration shown in Fig. 2(a) very much resembles the structure of the global minimum referred to as (S)-$I^-(H_2O)_6$ in Ref. 13 and also that corresponding to the stable $Y42$ structure of $(H_2O)_6^-$ found in Ref. 19. These features should be contrasted to those depicted in the central and bottom panels of Fig. 1 and in Figs. 2(b) and 2(c). Here $N_w=50$ clusters present ''intermediate'' solvation structures in which the iodide resides mostly within a $2.5\lesssim r\lesssim 7$ Å spherical shell, while for the largest aggregates, the most stable solvation states corresponds to inner states, characterized by $r\lesssim 3$ Å, a region that appears deprived from water molecules.

B. Electronic properties of I^-

Having established the main characteristics of the solvation structures of I^-, we will now consider the analysis of the electronic density of the excess charge. Figure 2 displays isodensity surfaces for the ground and first excited electronic states for typical $N_w=6$, 50, and 100 cluster configurations. Note that in all cases the ground-state density shows clear signs of *p*-like symmetry. While in the smallest aggregates a sizable fraction of the ground and first excited electronic densities spill out of the cluster ''boundaries,'' in larger clusters one observes a tighter confinement of the electronic density within the clusters. For example in $N_w=6$ clusters, typically 40% of the ground-state electronic density lies outside the spatial domain of the aggregates; this percentage practically vanishes for $N_w=50$ or 100. To quantify these observations in a more precise way, in Table II we present results for several relevant length parameters: We start by consider-

TABLE II. Solvation parameters for $I^-(H_2O)_n$. Distances are expressed in Å and time scales in ps.

n	$\sqrt{5/3}R_g$	$\langle\bar{r}_0\rangle$	$\mathcal{R}_0$	$\langle\bar{r}_1\rangle$	$\mathcal{R}_1$	τ_s
6	3.6	3.3	1.7	3.9	4.8	≈ 0.05[a]
50	7.3	4.7	1.7	4.6	3.9	0.19[b]
100	8.9	2.0	1.7	2.1	3.9	0.60[b]

[a]Computed only from the initial decay.
[b]Calculated from $S_E(t)$ up to 1 ps; after that time, a single-exponential decay was assumed.

ing the second column where we present the average cluster sizes as reflected by the radii of gyration, R_g:

$$R_g^2=\frac{1}{N_w}\sum_{i=1}^{N_w}(\mathbf{R}_{\mathrm{O}}^i-\mathbf{R}_{\mathrm{c.m.}})^2; \tag{9}$$

for reasonably spherical-like aggregates, the radius of the cluster can be roughly approximated by $\approx\sqrt{5/3}R_g$. In column 3, results for the average location of the electron within the cluster $\langle\overline{r_0}\rangle$, are displayed. The results were calculated from the following integral:

$$\langle\overline{r_n}\rangle=4\pi\int_0^\infty g_{\mathrm{c.m.}\text{-}\overline{r}_n}(r)r^3\mathrm{d}r, \tag{10}$$

where

$$g_{\mathrm{c.m.}\text{-}\overline{r}_n}(r)=\frac{1}{4\pi r^2}\langle\delta(|\overline{\mathbf{r}}_n-\mathbf{R}_{\mathrm{c.m.}}|-r)\rangle \tag{11}$$

and

$$\overline{\mathbf{r}}_n=\langle\psi_n|\hat{\mathbf{r}}|\psi_n\rangle. \tag{12}$$

The spatial extent of the electron is presented in the fourth column and can be readily estimated by computing $\mathcal{R}_0$, defined as

$$\mathcal{R}_n^2=\langle\psi_n|(\hat{\mathbf{r}}-\overline{\mathbf{r}}_n)^2|\psi_n\rangle. \tag{13}$$

From the simultaneous analysis of the entries of Table II and the profiles of $g_{\mathrm{c.m.}\text{-}\overline{\mathbf{r}}_n}(r)$ (also shown in Fig. 1) two important observations emerge: (i) The fact that the radial distributions $g_{\mathrm{c.m.}\text{-}\overline{\mathbf{r}}_0}$ are for all practical purposes similar to $g_{\mathrm{c.m.}\text{-I}}$ suggests that polarization effects arising from asymmetries of the local solvent electric fields seem to be negligible. This is not the case for the first excited electronic state—especially in small clusters—where the overall profiles of $g_{\mathrm{c.m.}\text{-}\overline{\mathbf{r}}_1}$ and consequently $\langle\overline{r_1}\rangle$ are shifted to greater distances. Of course, these asymmetry effects should diminish as we move to larger aggregates. (ii) The degree of electronic spill beyond the cluster ''boundaries'' is clearly indicated in the smallest cluster case, where we found that $\langle\overline{r_0}\rangle+\mathcal{R}_0>\sqrt{5/3}R_g$.

In Fig. 3 we display results for the density of bound states $D(E)$,

$$D(E)=\sum_{E_n<0}\langle\delta(E_n-E)\rangle. \tag{14}$$

The $N_w=6$ profile is dominated by a Gaussian-like profile centered at ≈-4.3 eV corresponding to the distribution of instantaneous ground states. By implementing standard projection operator techniques, we determined that these states exhibit an 80% of *p*-like character, the rest being of difficult symmetry characterization. In the vast majority of the configurations, we also found a second bound, highly diffuse, excited state [see Fig. 2(e)] at typical energies in the order of a few tenths of eV below the detachment threshold. This order of magnitude compares favorably well with VDE estimates of 0.038 eV and 0.069 eV obtained from more accurate quantum calculations of the (S)-$\mathrm{I}^-(\mathrm{H_2O})_6$ in Ref. 13. A similar projector analysis performed on these states failed to provide any clear prominent characterization of the wave function symmetry. Solvation in larger clusters leads to a gradual stabilization of the I^- ground state: The average ground-state energy drops to $\langle E_0\rangle\approx-6.2$ eV for $N_w=50$ and $\langle E_0\rangle\approx-6.8$ eV for $N_w=100$ aggregates. Compared to the $N_w=6$ case, the widths of the eigenstate distributions in the largest clusters show a moderate broadening, reflecting a larger variety of thermally accessible ambients available for ionic solvation within these aggregates. The characteristics of the excited electronic state distributions in larger aggregates exhibit a well-defined first-excited-state band located at ≈5 eV above the ground state, which represent CTTS precursor states. In addition we also found a quasicontinuum manifold of higher bound excited states near the detachment threshold energy.

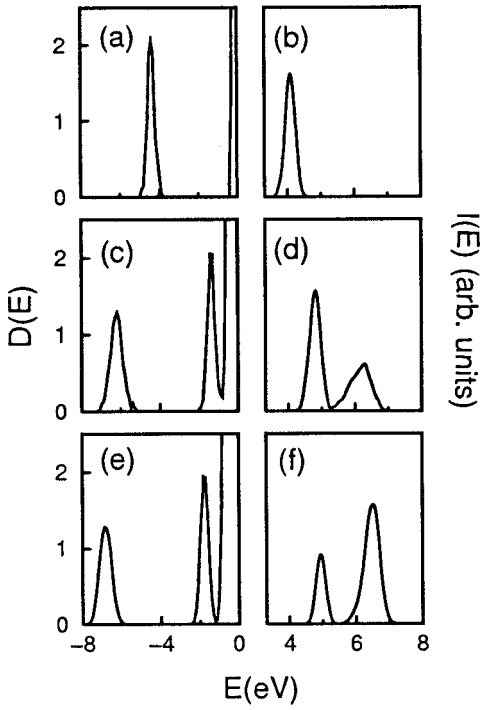

FIG. 3. Normalized density of states (left-hand panels) and absorption spectra (right-hand panels) for clusters of different sizes. $N_w=6$: (a), (b). $N_w=50$: (c), (d). $N_w=100$: (e), (f).

Ground-state absorption spectra $I(\omega)$ were computed within the Frank–Condon dipolar approximation as

$$I(\omega)\propto\omega(1-e^{-\beta\hbar\omega})\left\langle\sum_{i>0}\langle\psi_0|\hat{\boldsymbol{\mu}}|\psi_i\rangle^2\delta(\omega_{i0}-\omega)\right\rangle. \tag{15}$$

The results are shown in the right-hand side panels of Fig. 3. CTTS spectra are characterized by absorption peaks that present a gradual blueshift from 4 eV for $N_w=6$ to ≈4.85 eV for $N_w=50$ and 100. For the smallest clusters, the spectrum presents a single symmetric absorption maximum whose position agrees reasonably well with the excitation energy of the first CTTS precursor state reported in Ref. 13 as $h\nu_{\max}\approx3.7-4.4$ eV. In addition, a second peak corresponding to transitions to the manifold of higher bound excited states becomes more important as we move to larger aggregates.

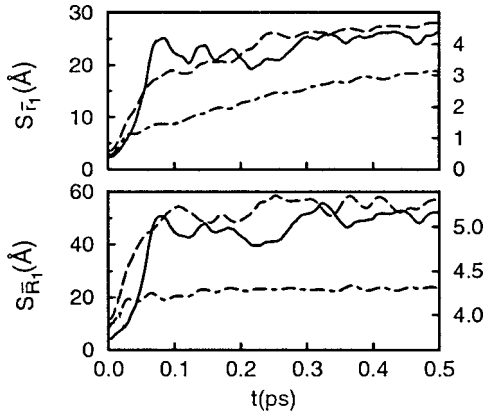

FIG. 4. Relaxation of the electron-iodine distance (top panel) and the electron wave function width (bottom panel) following the excitation of $I^-(H_2O)_n$. $n=6$: solid lines (left-hand axis). $n=50$: dashed lines (right-hand axis). $n=100$: dot-dashed lines (right-hand axis).

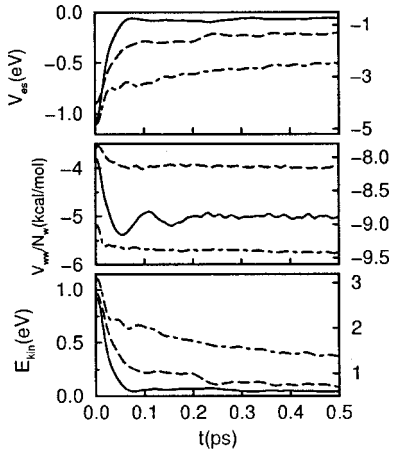

FIG. 5. Relaxation of the electron-water coupling (top panel), water-water interaction (middle panel), and electron kinetic energy (bottom panel) following the excitation of $I^-(H_2O)_n$. Same labeling as in Fig. 4.

IV. EXCITED-STATE DYNAMICS

We now turn to dynamical aspects of the photodetachment process. Our description will be based on the analysis of a series of nonequilibrium time correlation functions $S_O(t)$ for different relevant observables $O(t)$: namely,

$$S_O(t)=\langle O(t)\rangle_{\mathrm{ne}}, \tag{16}$$

where $\langle\cdots\rangle_{\mathrm{ne}}$ denotes an average sampled from a distribution of nonequilibrium initial conditions and the time origin was set to coincide with the vertical excitation. The most direct route to gain a preliminary qualitative insight of the detachment process is to consider $S_{\bar{\mathbf{r}}_1}$, the time evolution of the distance between the iodine and average position of the excited electron:

$$S_{\bar{\mathbf{r}}_1}(t)=\langle|\bar{\mathbf{r}}_1(t)-\mathbf{R}_I(t)|\rangle_{\mathrm{ne}}. \tag{17}$$

Results for $S_{\bar{\mathbf{r}}_1}$ computed from an ensemble of 100 relaxations are shown in the top panel of Fig. 4. We observe that the curves exhibit two well-differentiated temporal regimes. The $N_w=6$ case is perhaps the clearest: During the first 100 fs, the center of the excess charge separates $\approx$25 Å away from the iodine, a distance far beyond the cluster boundaries. Note that during this brief time interval, the position of the much heavier iodine should remain practically unchanged, so the results reflect exclusively electronic dynamics. This fast initial displacement is followed by a much slower diffusive-like motion that dominates the long-time behavior of the electron detachment. In intermediate- and large-size domains, the stronger confining characteristics of the potential generated by the classical bath diminish the magnitude of the initial separation. Although the distinction between the two temporal regimes becomes somewhat less sharp, changes in the slope of the electron displacement from the iodine at $t\approx50$ and 25 fs are still perceptible in the $N_w=50$ and 100 curves, respectively. For these larger aggregates, $S_{\bar{\mathbf{r}}_1}(t)$ at longer times (not shown) levels off at distances comparable to the cluster size. At this stage we cannot assert whether these plateaulike behaviors are due to finite-size effects imposed by the cluster free surface or to a solvation stabilization similar to that found in bulk phases at similar distances.[23]

The analysis of the time evolution of the spatial extent of the electron described in terms of $S_{\mathcal{R}_1}(t)$ is also instructive; the results are displayed in the bottom panel of Fig. 4. Note that the overall relaxations of $\mathcal{R}_1(t)$ are qualitatively similar to those of $\bar{\mathbf{r}}_1$. Here, again, changes in small clusters are the most evident: During the first 100 fs, the electron density, initially distributed over domains of typical size $\approx$5 Å (see column 6 of Table II), exhibits a fast spread attaining $\approx$40 Å. Considering the highly diffuse nature of the electronic density upon excitation, results for the long-time behavior of $S_{\mathcal{R}_1}(t)$ in these small aggregates are likely to be affected by non-negligible errors, due the poor description provided by the adopted Gaussian basis set. The results as such should only be taken as qualitative indicators of the order of magnitude of the limiting, $t=\infty$, electron size and position. Results for larger clusters show a more moderate electron delocalization transient that takes place exclusively during the early stages of the detachment process; this would indicate that during the subsequent diffusive motion away from the iodine, the electron is already fully thermalized.

Energetic relaxations provide complementary information that permits a more complete understanding of the overall relaxation processes. The top panel of Fig. 5 depicts results for the time relaxations of the electron-solvent coupling. Note that upon excitation the electronic solvation becomes less favorable, mainly due to the more delocalized nature of the excess charge. The less favorable electronic solvation should be contrasted with the gradual stabilization of the—usually competing—water-water interactions shown in the middle panel, which reflects the gradual buildup of a stronger hydrogen bond network. Similarly, basic quantum mechanical arguments can be invoked to rationalize the reduction of the electronic kinetic energy shown in the bottom panel in terms of the larger spatial extent of the detached electron.

In bulk phases, explicit dynamical information about the solvation process can be obtained from time-dependent

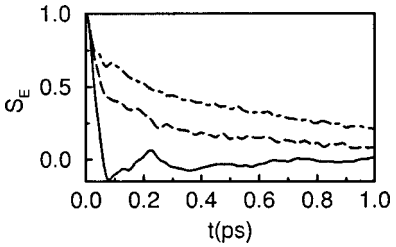

FIG. 6. Normalized relaxation of the solvent energy gap (see text). Same labeling as in Fig. 4.

Stokes shifts of fluorescent cromophores.[24] In computer simulations, the most direct route to describe the dynamics is by considering the normalized nonequilibrium response of the solvent defined by[25]

$$S_{\mathrm{E}}(t)=\frac{\langle \Delta E(t)-\Delta E(\infty)\rangle_{\mathrm{ne}}}{\langle \Delta E(0)-\Delta E(\infty)\rangle_{\mathrm{ne}}}; \tag{18}$$

where $\Delta E(t)=E_1(t)-E_0(t)$ represents the instantaneous solvent energy gap. In Fig. 6 we present results for $S_{\mathrm{E}}(t)$. The profiles show two interesting features: (i) In large aggregates, they retain the bimodal character observed in bulk polar media, i.e., a fast, inertial transient that characterizes the early stages of the solvation (typically taking place during the first hundreds of femtoseconds) and accounting for a large fraction of the overall solvation response, followed by a much slower, diffusive regime with a characteristic time scale of the order of 1–5 ps. (ii) The clear prominence of the inertial regime in small clusters diminishes as we move to larger aggregates. In fact, for $N_w=6$ the relaxation is characterized by a unique fast relaxation lasting $\approx$50 fs.

A reasonable estimate of the overall time scale involved in the solvation process can be obtained from the average correlation time τ_s, defined as

$$\tau_s=\int_0^\infty S_{\mathrm{E}}(t)\mathrm{d}t. \tag{19}$$

The entries in the last column of Table II reveal that the solvation relaxation is approximately one order of magnitude slower in $N_w=100$ than in $N_w=6$ clusters. The reasons for such a disparity in the time scales can be found in the observation referred to as (ii) in the previous paragraph and in the increasing contribution to the total relaxation arising from the diffusive branch as we move to larger aggregates. Two different types of motion take place during this stage: first, a reorganization of the spatial distribution of the water molecules favoring a stronger intramolecular connectivity via new hydrogen bonds in detriment of the solvation of the excited electron and, second, the gradual diffusive detachment of the electron away from the iodine. Of course, contributions from the latter motion should relax at a faster rate in smaller clusters, where full detachment between the iodine and electron is partially prevented by the spatial restrictions imposed by the size of the aggregate.

V. CONCLUSIONS

The results presented in this paper provide new insights into equilibrium and dynamical aspects of electron photodetachment reactions in small water clusters. Our main objective focused on assessing the effects of thermal and polarization fluctuations provided by three cluster environments with different extents of spatial confinement, on the microscopic mechanisms that drive the reaction. These fluctuations, in turn, determine the characteristics of the electron localization and the subsequent detachment following photoexcitation of the probe. In this first approach to the problem, we incorporated only the basic ingredients that would allow us to acquire a reasonable, qualitative description of the solvation dynamics. Consequently, no efforts have been made at this stage to perform a detailed analysis of possible choices for the different Hamiltonian parameters. The mixed quantum-classical approach that we adopted included two main approximations: (i) Quantum fluctuations were described exclusively in terms of a simplified one-electron-coupled-to-a-classical-bath model; (ii) The dynamics of the classical nuclei was computed within the adiabatic approximation. As such, our simulation experiments predict a gradual transition from *surface*- to *bulk*-like solvation states for the I^- as we move from $N_w=6$ to $N_w=100$. The transition between these limiting solvation states leads to a gradual stabilization of the ground and manifold of excited electronic states and also to a gradual blueshift in the corresponding absorption spectra, in agreement with experimental results.

From the dynamical point of view, the excitation of the probe in $N_w=6$ aggregates generates highly diffuse electronic states with typical sizes of $\approx$20–30 Å; these electrons remain weakly attached to the cluster surface, with typical binding energies in the order of a few tenths of eV. The charge delocalization induces a weaker electron-solvent coupling and promotes an overall reorganization in the solvent characterized by a stronger intramolecular hydrogen bond network. The whole solvent relaxation process requires 0.05–0.1 ps. In larger aggregates, the extent of the initial electron delocalization is drastically reduced, and the subsequent diffusive adiabatic detachment of the electron from the iodine exhibits characteristics similar to those found in conventional macroscopic phases.[10] In the case of $N_w=100$ clusters, the solvent reorganization is significantly slower and requires 0.6 ps.

Finally, we would like to point out that, regardless the specific cluster size considered, we found no evidence of relaxation channels involving either electronic stabilization via solvation or isomerization transitions between two different stable solvation states. These results clash with experimental evidence of time-dependent VDE measurements in $N_w=6$ clusters.[15] Although the reasons for such discrepancies remain obscure to us, we can speculate on a few plausible reasons to account for the lack of agreement. The particular choice for the Hamiltonian is perhaps one of the first points that should deserve further investigation: The TIP4P model has proved to be well suited to describe structures and energetics of small aqueous clusters;[26] however, in systems involving excess charges, it may turn out to be too ''hydrophilic'' and not properly balanced by the electron-water and electron-iodine effective interactions adopted here. In this respect, although we put special effort in optimizing the parameterization of the latter interactions so as to obtain rea-

sonable agreement with more elaborate quantum calculations, our very much simplified one-electron model might still yield a rather poor description of highly diffuse, excited electronic states. The absence of polarization effects in the solvent is also a second aspect that will require additional analysis. The sudden changes in the electronic density of the solute are likely to be followed by strong polarization fluctuations, particularly in the case of small aggregates. We note that a few exploratory test runs using the fluctuating charge model by Rick, Stuart, and Berne[27] failed to provide a stable dynamics of the partial charges in small clusters—possibly due to the exceedingly large energy gap between the ground and first excited states of the probe—and furthermore, did not show any qualitative change in the solvation responses of the larger aggregates. The validity of the quantum adiabatic dynamics hypothesis for the nuclei and the possibility of new relaxation channels involving nonadiabatic transitions is another point to be taken into consideration. In bulk phases, besides the usual adiabatic detachment process, transitions between different Born-Oppenheimer surfaces may lead to nonadiabatic tunneling in which electrons are transferred directly to the solvent without the involvement of a CTTS state.[8] At this point, the importance of the effects arising from these kinds of nonadiabatic transitions in cluster environments is of difficult prediction. Investigations along these directions are currently being undertaken in our laboratory and will surely provide new answers in clarifying these controversial issues.

ACKNOWLEDGMENTS

Partial financial support from Fundación Antorchas of Argentina is very much appreciated. M.D.E. is a recipient of support from CONICET. D.L. is a staff member of CONICET.

[1] J. Jortner and A. Treinin, Trans. Faraday Soc. **58**, 1053 (1962); J. Jortner, M. Ottolenghi, and G. Stein, J. Chem. Phys. **68**, 247 (1964).
[2] M. J. Blandamer and M. F. Fox, Chem. Rev. **70**, 59 (1970), and references therein.
[3] F. H. Long, H. Lu, and K. B. Eisenthal, J. Chem. Phys. **91**, 4193 (1989); F. H. Long, H. Lu, X. Shi, and K. B. Eisenthal, Chem. Phys. Lett. **169**, 165 (1990); F. H. Long, H. Lu, and K. B. Eisenthal, Phys. Rev. Lett. **64**, 1469 (1990).
[4] Y. Gauduel, H. Gelabert, and M. Ashokkumar, Chem. Phys. **197**, 167 (1995); M. Ashokkumar, J. Gelabert, A. Antonetti, and Y. Gauduel, in *Ultrafast Reaction Dynamics and Solvent Effects*, edited by Y. Gauduel and P. J. Rossky (AIP, New York, 1993).
[5] J. A. Kloepfer, V. H. Vilchiz, V. A. Lenchenkov, and S. E. Bradforth, Chem. Phys. Lett. **298**, 120 (1998).
[6] W.-S. Sheu and P. Rossky, J. Am. Chem. Soc. **115**, 7729 (1993).
[7] W.-S. Sheu and P. Rossky, Chem. Phys. Lett. **202**, 186 (1993).
[8] W.-S. Sheu and P. Rossky, Chem. Phys. Lett. **213**, 233 (1993).
[9] W.-S. Sheu and P. Rossky, J. Phys. Chem. **100**, 1295 (1996).
[10] A. Staib and D. Borgis, J. Chem. Phys. **103**, 2642 (1995); Chem. Phys. Lett. **230**, 405 (1994); J. Chem. Phys. **104**, 9027 (1996).
[11] D. Serxner, C. E. H. Dessent, and M. A. Johnson, J. Chem. Phys. **105**, 7231 (1996).
[12] J. E. Combariza, N. R. Kestner, and J. Jortner, Chem. Phys. Lett. **203**, 423 (1993); J. Chem. Phys. **100**, 2851 (1994); Chem. Phys. Lett. **221**, 156 (1994).
[13] H.-Y. Chen and W.-S. Chen, J. Am. Chem. Soc. **122**, 7534 (2000).
[14] H. M. Lee and K. S. Kim, J. Chem. Phys. **114**, 4461 (2001).
[15] L. Lehr, M. T. Zanni, C. Frischkorn, R. Weinkauf, and D. M. Newmark, Science **284**, 635 (1999).
[16] C. Frischkorn, M. T. Zanni, A. V. Davis, and D. M. Newmark, Faraday Discuss. **115**, 49 (2000).
[17] W. L. Jorgensen, J. Chandrasekhar, J. D. Madura, R. Impey, and M. L. Klein, J. Chem. Phys. **79**, 926 (1983).
[18] M. Sprik and M. L. Klein, J. Chem. Phys. **87**, 5987 (1987); **89**, 1592 (1988).
[19] S. Lee, J. Kim, S. J. Lee, and K. S. Kim, Phys. Rev. Lett. **79**, 2038 (1997).
[20] A mobile basis set centered at the instantaneous maxima of the electronic density has been used in the bulk simulations reported in Ref. 10.
[21] Surface and bulk solvation states have been found in simple ions dissolved in water clusters. For recent studies, see L. Parera and M. L. Berkowitz, J. Chem. Phys. **95**, 1954 (1991); **96**, 8288 (1992); W. L. Jorgensen and D. L. Severance, *ibid.* **99**, 4233 (1993); L. X. Dang and D. E. Smith, *ibid.* **99**, 6950 (1993); L. Parera and M. L. Berkowitz, *ibid.* **99**, 4236 (1993); L. X. Dang and B. C. Garret, *ibid.* **99**, 2972 (1993); L. X. Dang, *ibid.* **110**, 1526 (1999); D. J. Tobias, P. Jungwirth, and M. Parrinello, *ibid.* **114**, 7036 (2001).
[22] There seems to persist some minor inconsistencies between photoelectron spectroscopy and computer simulation results. See G. Markovich, R. Giniger, M. Levin, and O. Chesnovsky, J. Chem. Phys. **95**, 9416 (1991); G. Markovich, S. Pollak, R. Giniger, and O. Chesnovsky, *ibid.* **101**, 9344 (1994).
[23] Stable electron-chlorine ion pairs in bulk water have been reported by D. Borgis and A. Staib, J. Chem. Phys. **104**, 4776 (1996).
[24] For recent articles on solvation dynamics in bulk polar phases, see M. Maroncelli, J. Mol. Liq. **57**, 1 (1993); M. Maroncelli, P. V. Kumar, A. Papazyan, M. L. Horng, S. J. Rosenthal, and G. R. Fleming, in *Ultrafast Reaction Dynamics and Solvent Effects*, edited by Y. Gauduel and P. J. Rossky (AIP, New York, 1993); G. R. Fleming, *Chemical Applications of Ultrafast Spectroscopy* (Oxford University Press, New York, 1986).
[25] B. M. Ladanyi, in *Theoretical Methods in Condensed Phase Chemistry*, edited by S. D. Schwartz (Kluwer Academic, Dordrecht, 2000).
[26] J. Rodriguez, D. Laria, E. J. Marceca, and D. A. Estrin, J. Chem. Phys. **110**, 9039 (1999).
[27] S. W. Rick, S. J. Stuart, and B. J. Berne, J. Chem. Phys. **101**, 6141 (1994).